JOURNAL OF GEOPHYSICAL RESEARCH, VOL. 102, NO. C10, PAGES 23,145–23,153, OCTOBER 15, 1997

Defining and quantifying microscale wave breaking with infrared imagery

A. T. Jessup and C. J. Zappa
Applied Physics Laboratory, College of Ocean and Fishery Sciences, University of Washington, Seattle

Harry Yeh
Department of Civil Engineering, University of Washington, Seattle

Abstract. Breaking without air entrainment of very short wind-forced waves, or microscale wave breaking, is undoubtedly widespread over the oceans and may prove to be a significant mechanism for enhancing the transfer of heat and gas across the air-sea interface. However, quantifying the effects of microscale wave breaking has been difficult because the phenomenon lacks the visible manifestation of whitecapping. In this brief report we present limited but promising laboratory measurements which show that microscale wave breaking associated with evolving wind waves disturbs the thermal boundary layer at the air-water interface, producing signatures that can be detected with infrared imagery. Simultaneous video and infrared observations show that the infrared signature itself may serve as a practical means of defining and characterizing the microscale breaking process. The infrared imagery is used to quantify microscale breaking waves in terms of the frequency of occurrence and the areal coverage, which is substantial under the moderate wind speed conditions investigated. The results imply that "bursting" phenomena observed beneath laboratory wind waves are likely produced by microscale breaking waves but that not all microscale breaking waves produce bursts. Oceanic measurements show the ability to quantify microscale wave breaking in the field. Our results demonstrate that infrared techniques can provide the information necessary to quantify the breaking process for inclusion in models of air-sea heat and gas fluxes, as well as unprecedented details on the origin and evolution of microscale wave breaking.

1. Introduction

The role of deep water wave breaking in limiting wave growth and as a source of turbulent mixing has motivated a rich and continuing history of research on the importance of breaking waves in air-sea interaction [*Banner and Peregrine*, 1993; *Thorpe*, 1995; *Melville*, 1996]. In general, wave breaking is the process by which a portion of the fluid near a wave crest overtakes the form of the wave, becomes turbulent as it spills down the forward slope, and ultimately leaves behind a decaying turbulent wake. In this context, breaking waves that entrain air and thereby produce whitecaps are simply the most intense and visibly obvious type of a phenomenon that occurs over a wide range of scales. *Banner and Phillips* [1974] coined the term "microbreaking" to describe the breaking of very short gravity waves without air entrainment, noting that microbreaking, or microscale breaking, is far more widespread than whitecapping. The widespread occurrence of microscale wave breaking suggests that its cumulative effect on the fluxes of heat and gas across the air-sea interface may be significant, especially for moderate wind speeds [*Banner and Peregrine*, 1993; *Melville*, 1996].

Low visual contrast due to the absence of air entrainment makes microscale breaking waves difficult to identify, while their small scale makes quantitative measurements especially challenging. The diagram and video image in Figure 1 illustrate the typical features of microscale breaking waves. The defining characteristic is a bore-like crest accompanied by parasitic capillary waves distributed along the forward face. Microscale breaking waves are typically described as $O(0.1–1)$ m in length and a few centimeters in amplitude. In laboratory wind wave studies, *Okuda* [1982] and *Ebuchi et al.* [1987] identified a "high-vorticity region" near the crests of gravity waves with capillary ripples generated ahead of the crests. The origin of vorticity within this surface "roller" has been identified by *Longuet-Higgins* [1992] as the accompanying parasitic capillaries, which themselves generate fluid rotation (i.e., vorticity) via the surface-tension effect [*Yeh*, 1992, 1995]. Rollers [*Longuet-Higgins*, 1992], breaking wavelets [*Csanady*, 1990], and steep wind waves accompanied by a high-vorticity layer near the crest [*Okuda*, 1982] are all descriptions of phenomena which are clearly identified with the microbreaking described by *Banner and Phillips* [1974]. For consistency and convenience, we adopt the general description of breaking offered above and use "microscale breaking waves" to describe very short, wind-generated gravity waves which break without entraining air.

Since breaking waves of all scales disrupt the diffusive sublayer which regulates the flux of gas across the air-sea interface, near-surface turbulence generated by wave breaking has been proposed as a significant mechanism for air-water gas transfer. *Kitaigorodskii* [1984] submitted that the gas transfer rate is determined primarily by large-scale breaking waves that produce whitecaps. *Csanady* [1990], on the other hand, argued that gas transfer is controlled by microscale breaking waves, especially

Paper number 97JC01449.
0148-0227/97/97JC-01449$09.00

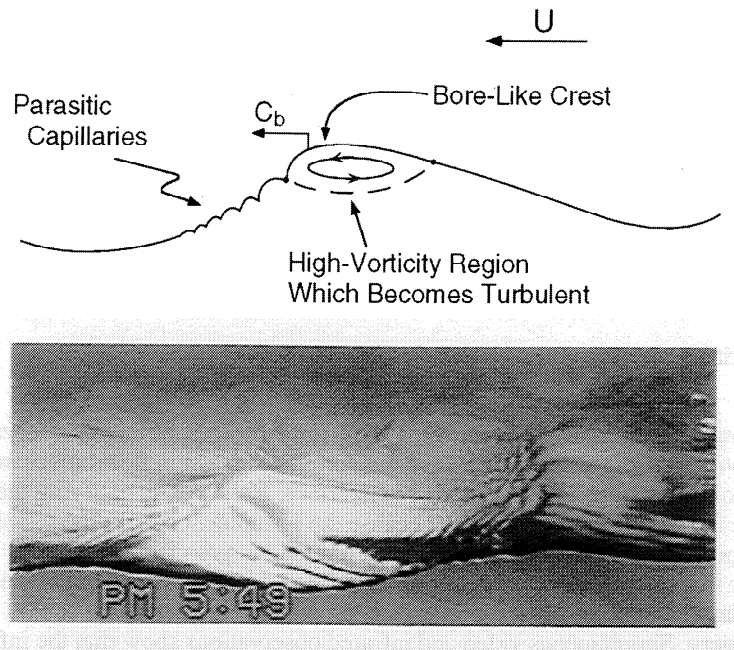

Figure 1. (top) The characteristic feature of a microscale breaking wave is a bore-like crest with parasitic capillary waves riding along the forward face; U is the wind speed, and C_b is the crest speed of the microscale breaking wave. (Adapted from *Ebuchi et al.* [1987].) (bottom) Video image of a microscale breaking wave with a wavelength of roughly 0.1 m.

under conditions of moderate wind speed. Here we present new and intriguing measurements showing that microscale breaking waves produce thermal surface signatures that are consistently detected by infrared imaging techniques. Evidence from the literature suggests that the microscale breaking waves responsible for these thermal events are the source of the turbulent "bursting" structures observed beneath laboratory wind waves. The conceptual model we present, which explains our infrared observations, suggests that thermal detection of microscale wave breaking may serve as a de facto definition of the phenomenon itself. Our results demonstrate that infrared techniques can provide the information necessary to quantify microscale breaking in order to determine its role in the exchange of heat and gas across the air-sea interface. Furthermore, infrared techniques should provide unprecedented details on the origin and evolution of microscale wave breaking.

2. Infrared Signature of Microscale Wave Breaking

Under most circumstances, a net upward heat flux from the ocean occurs primarily by molecular conduction through a thermal boundary layer, or skin layer, at the ocean surface. As a result, the "skin temperature" at the top of this layer is a few tenths of a degree Celsius cooler than the bulk temperature immediately below the skin layer [*Katsaros*, 1980; *Robinson et al.*, 1984] . The conceptual model in Figure 2 portrays the disruption of this cool skin layer by a microscale breaking wave. Turbulence generated by the breaking process momentarily disrupts the skin layer and transports warmer water from below to the free surface such that the skin temperature within the resulting turbulent wake is approximately equal to the bulk temperature. As the turbulent wake subsides, the surface cools, and the skin temperature returns to its original value at a rate which increases with increasing ambient heat flux [*Jessup et al.*, 1995]. Detection of infrared radiation provides a remote measurement of the skin temperature since the optical depth, about 10 μm, is at least one order of magnitude less than the skin layer thickness. An infrared imager therefore is ideally suited to detect and quantify the renewal of surface water by individual microscale breaking events.

In the course of a recent laboratory study focusing on large-scale breaking [*Jessup et al.*, 1995, 1997] limited measurements of wind-generated waves (in the absence of large-scale breaking) revealed the infrared signature of microscale breaking waves. Because this experiment at the Canada Centre for Inland Waters (CCIW) in Burlington, Ontario, was not specifically designed to study microscale wave breaking, the quantitative measurements

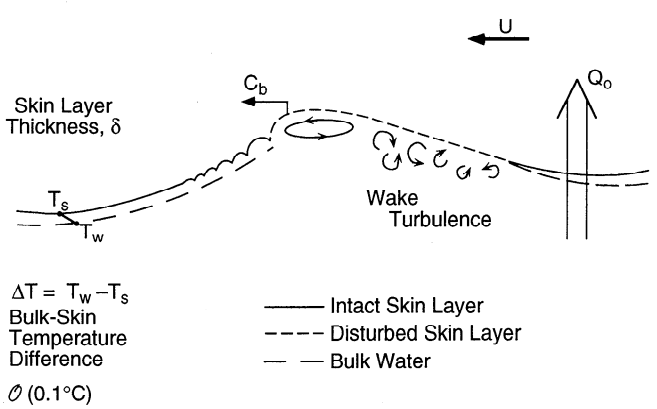

Figure 2 Conceptual model of disruption of the cool skin layer by a microscale breaking wave which leads to the thermal signature detectable by infrared imaging. The cool skin is disrupted and replaced by warmer bulk fluid from below. The bulk – skin temperature difference, ΔT, across the cool skin layer of thickness δ is supported by the net heat flux, Q_o [*Saunders*, 1967].

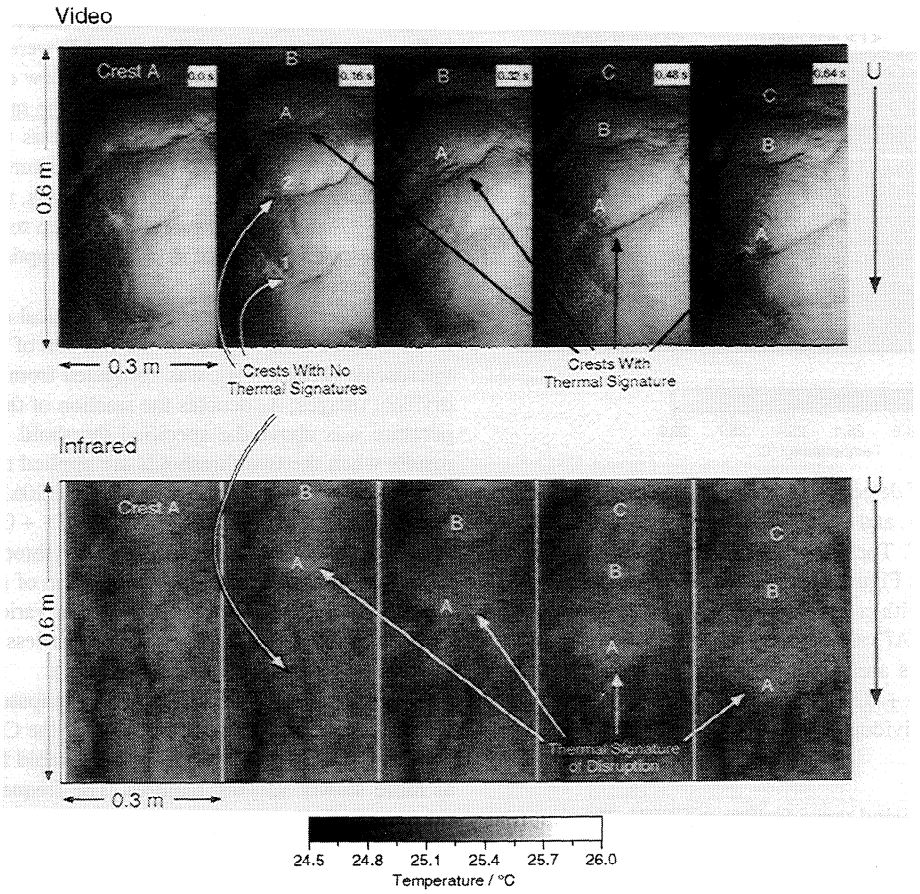

Figure 3. Simultaneous (top) video and (bottom) infrared images of wind waves in the University of Washington wave tank. Thermal features in the infrared images, taken with an Agema model 880 LW imager, are clearly associated with the wave crests labeled A–C in the video images and thus qualify as microscale breaking waves according to the conceptual model of Figure 2. Note that the crests labeled 1 and 2 have no detectable thermal signature, implying that not all waves are breaking. The bulk water temperature T_w was 25.8°C, the air – water temperature difference ΔT_{aw} was –7.3°C, the relative humidity RH was 53%, the frequency of the dominant wave f_p was 3.44 Hz (measured at the test section), and the wind speed U was 6.3 m s^{-1}.

available at this time are for a narrow range of conditions. Furthermore, the video recordings made at CCIW were inadequate to present visual details of the microscale breaking process. To provide quality flow visualization for this report, we have supplemented the CCIW measurements with video and infrared measurements taken under comparable conditions in a wind wave tank at the University of Washington (UW). The CCIW wave tank measured 10 m long, 0.3 m wide, and 0.4 m deep, while the UW tank measured 10 m × 1.2 m × 0.9 m.

Figure 3 shows a sequence of simultaneous, colocated video and infrared images of wind waves taken at the UW facility. The sensors were directed at the surface at an incidence angle of 30°, the image size is roughly 0.6 m × 0.3 m, and the time between images is 0.16 s. The infrared measurements were made using an infrared imager (Agema model 880 LW) operating at wavelengths of 8–12 μm. The manufacturer's specification of noise equivalent temperature difference is 0.05 °C. The wind speed was 6.3 m s^{-1} at a fetch of 5 m, and the wind direction in the figure is from top to bottom. Wave crests appear as dark, roughly horizontal lines in the video image. A crescent-shaped patch of higher temperature appears at the top of the first infrared image; this patch corresponds to the wave front labeled A in the first video image. This patch grows and propagates down the tank as wave front A continues to disrupt the thermal boundary layer. Fainter warm patches corresponding to the crests that follow A in the video images (labeled B and C) are also evident in the infrared images. These signatures are typical of the infrared manifestations of microscale breaking that we have observed. As in this example, we have noticed that successive crests tend to break periodically in a manner suggestive of wave breaking in groups [*Donelan et al.*, 1972] . Note that the individual crests labeled 1 and 2 in the video images do not show a corresponding thermal signature, implying that only a portion of the waves qualify as microscale breaking events. This observation suggests that the infrared signature of wave-induced skin layer disruptions may be used to define microscale wave breaking. Also apparent in the bottom of the infrared images are dark streaks aligned with the wind direction. These features generally persist much longer than the wave period and may be an indication of secondary circulation related to the waves [*Gemmrich and Hasse*, 1992].

We performed a simple thresholding analysis to demonstrate the capability of infrared techniques to quantify the fraction of surface area affected by these microscale breaking events. The analysis was performed on infrared imagery similar to that in Fig-

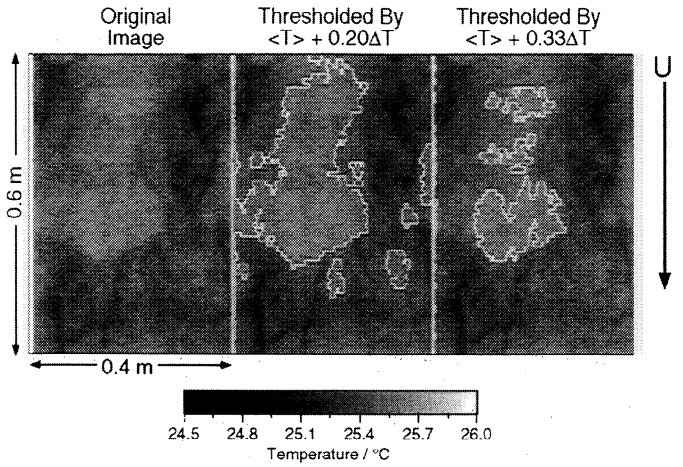

Figure 4. Example of detection technique based on the mean surface temperature, $\langle T \rangle$, and the bulk – skin temperature difference for the entire run, ΔT. The image on the left is the same as the fifth infrared image in Figure 3 except that the horizontal scale is now 0.4 m. Areas with a temperature greater than the lower threshold ($\langle T \rangle + 0.20\Delta T$) are outlined in the middle image, while the right image shows areas with temperature greater than the higher threshold ($\langle T \rangle + 0.33\Delta T$). Note that the higher threshold identifies the three individual events labeled A–C in Figure 3.

ure 3 but taken in the wind-wave facility at CCIW. The four runs of experimental data analyzed here consist of images taken at a rate of 25 Hz for a period of 300 s each. The wind speed was constant at approximately 5 m s^{-1} at a fetch of 6 m. The heat flux was varied by controlling the air – water temperature difference while the relative humidity remained steady at 64%. Temperature thresholds based on the mean surface temperature, $\langle T \rangle$, and the bulk – skin temperature difference, ΔT, were used to identify the disrupted area (taking into account the slow decrease in $\langle T \rangle$ over the course of the run due to cooling). The mean bulk – skin temperature difference, ΔT, was computed as the mean difference between the maximum and mean temperatures within the images over the course of the run. For this analysis, thresholds of $0.20\Delta T$ and $0.33\Delta T$ above the mean were chosen to outline the features that correspond to areas of skin layer disruption due to microscale breaking events.

After a series of standard morphological operations to reduce noise effects, a time series of the fraction of the area affected by microscale breaking, A_b, was computed from the sequence of individual images; A_b denotes the fraction of the image whose temperature was above the specified threshold. Figure 4 shows the results when the two thresholds are applied to the fifth image of Figure 3. The lower threshold ($\langle T \rangle + 0.20\Delta T$) detects one large event, whereas the higher threshold ($\langle T \rangle + 0.33\Delta T$) successfully separates three events identified with the three individual crests in Figure 3. Although this simple definition of fractional area averages out the effect of multiple events in various stages of development within a single image, A_b nonetheless provides a measure of the areal extent of microscale breaking.

Figure 5 shows time series of A_b computed using the chosen thresholds for one run measured during the CCIW laboratory experiment. Both time series show large, rapid fluctuations, as well as more slowly varying features. The frequency of the fluctuations depends on the recovery rate of the skin layer, the occurrence of multiple breaking events within the image, and the time between the events. For the run shown in Figure 5, the mean fraction of disrupted area is 0.35 for the lower threshold and 0.19 for the higher threshold, indicating that a significant fraction of the surface is disrupted on a continuous basis. For the four runs at

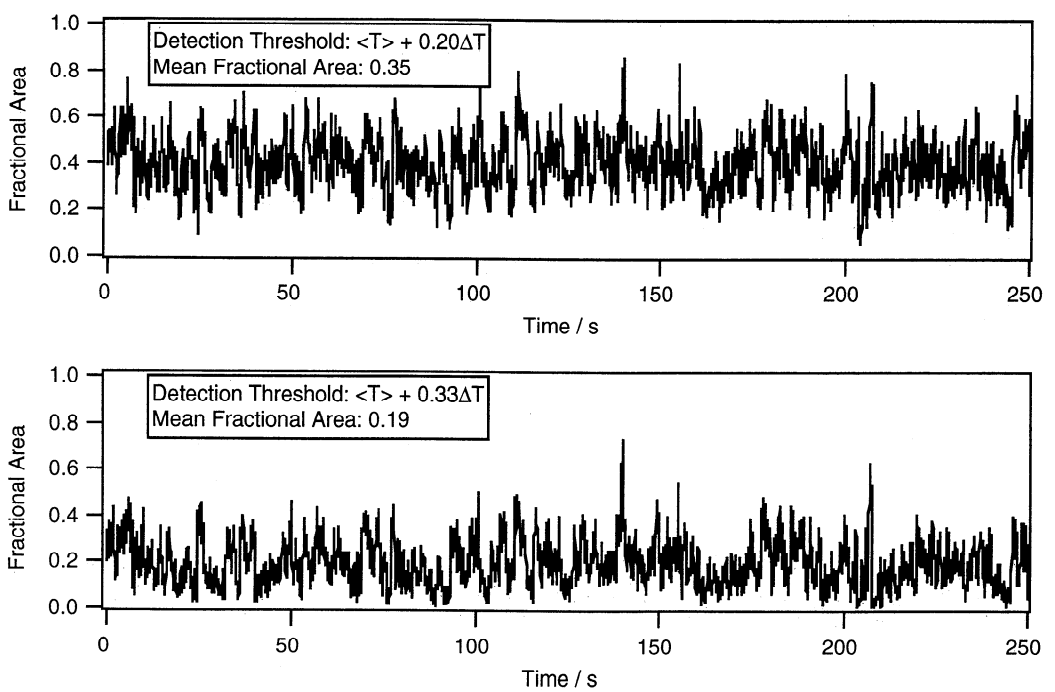

Figure 5. Time series of A_b, the fractional area of microscale wave breaking, detected when using (top) the lower threshold (mean $A_b = 0.35$) and (bottom) the higher threshold (mean $A_b = 0.19$). Data were taken during an experiment at the Canada Center for Inland Waters (CCIW); $T_w = 26.8°C$, $\Delta T_{aw} = -1.7°C$, RH = 65%, $f_p = 3.28$ Hz (measured 1 m downwind of the test section), and $U = 5.0$ m s^{-1}.

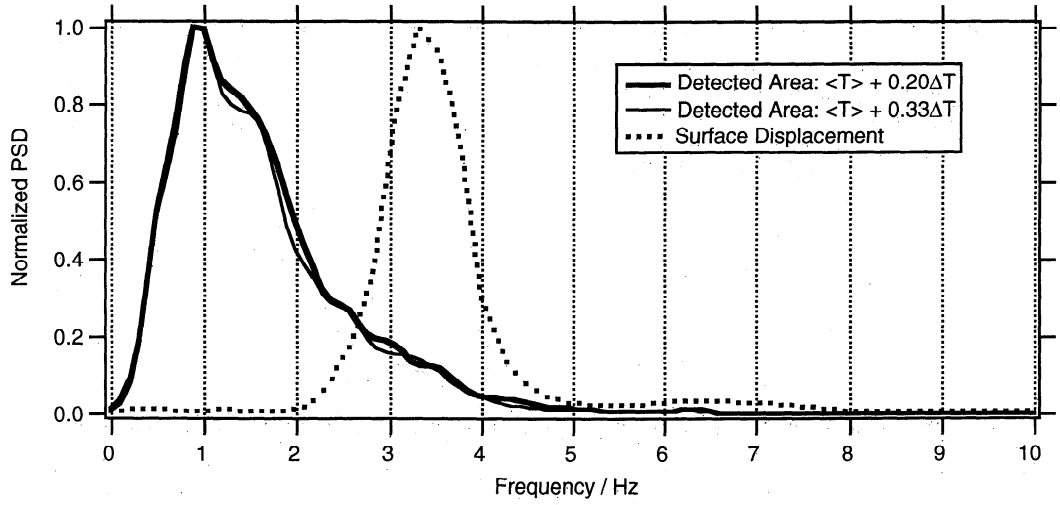

Figure 6. Comparison of normalized power spectra of surface displacement and fractional area A_b for the run in Figure 5 using the same threshold levels. The dominant frequency of A_b provides a measure of the frequency of occurrence of microscale wave breaking and is roughly one-third the dominant wave frequency.

constant wind speed and relative humidity considered here, the average A_b did not change (within ± 0.01) as the air – water temperature difference was varied from –1.7°C to –9.1°C (corresponding to an increase in ΔT from 0.16°C to 0.36°C).

In order to evaluate how often the detected events occurred, we computed power spectra from the time series of A_b derived from the threshold analysis described above. The dominant frequency of A_b provides a measure of the frequency of occurrence of the disturbances due to microscale breaking, even though multiple events may be detected in a single image. Figure 6 compares the normalized power spectra of A_b with the normalized spectrum of the surface displacement measured 1 m downwind of the imaged area. The dominant frequency of A_b is roughly one-third the dominant wave frequency for all four runs at this wind speed of 5 m s^{-1}. Similarly, power spectra of the surface temperature for a single point at random locations also show a frequency roughly one third of the wave frequency, implying that one wave out of three breaks.

Details on the origin and evolution of the surface disruption near the crest of microscale breaking waves are revealed by operating the imager in a "line scan" mode which provides a scan along the same line at a rate of 2500 Hz. An example of the high temporal and spatial resolution available using this rapid sampling capability is shown in the infrared space-time plot in Figure 7, which also shows corresponding video images. The vertical axis is the distance along the tank over which the imager scans, and the white line in each video frame corresponds to the location of the scan line. The horizontal axis in the space-time plot spans a duration of 0.9 s, with each vertical line denoting the time of a video frame. The propagation down the tank of the microscale breaking crests labeled E and F in the video images corresponds to the light-colored, steeply sloping bands labeled E and F in the infrared space-time plot. The slopes of these bands determine the speed of the thermal features which, at 0.5 m s^{-1}, matches the phase speed of the dominant wave. Fine streaky signatures of surface drift features move at a much slower velocity (3% to 4% of the wind speed U) and correspond to the motion of the patchy features near the bottom of the infrared images in Figure 3. Note that the slope of the surface drift features tends toward zero just ahead of the sloped line corresponding to breaking crest E, indicating the occurrence of a region of very small or no drift.

Recent measurements aboard R/P *Flip* provided an opportunity to observe microscale wave breaking in a field setting. Figure 8 shows two nighttime sequences of infrared images depicting examples of the disruption of the thermal boundary layer by microscale wave breaking. These disruptions produced temperature changes of 0.1°C, which were comparable to ΔT measured independently. The imager was mounted 8 m above the still-water level and directed toward the surface at an incidence angle of 30°. The image size is roughly 1 m × 0.75 m, and the time between images is 0.12 s. The wind speed measured at a height of 10 m, U_{10}, was roughly 6.6 m s^{-1} during the top sequence and 5.7 m s^{-1} during the bottom; the wind direction for both is from top to bottom. The significant wave height (SWH) measured 2.28 m in the top sequence and 2.14 m in the bottom, with peak swell frequencies, f_{ps}, of 0.070 Hz and 0.074 Hz respectively. The microscale breaking events have been thresholded and outlined in a manner similar to that used in Figure 4. The top sequence depicts the evolution of a single event labeled J followed by the inception of a second event labeled K, while the bottom sequence shows multiple events throughout. In both cases the microscale breaking appeared to occur as the orbital motion of long waves augmented the surface drift. This description is suggestive of the mechanism proposed and measured in the laboratory by *Phillips and Banner* [1974] in which the increased surface drift due to longer waves leads to microscale wave breaking.

3. Discussion

Organized, turbulent structures, or bursts, in the air and water associated with wind waves which do not produce air entrainment have been documented in a variety of laboratory studies over the past two decades. *Toba et al.* [1975] described a downward, subsurface flow associated with the surface convergence near the bore-like crests of steep wind waves. These downward bursts have been related to flow separation and reattachment in the air that occur near the wave crests [*Kawamura and Toba*, 1988]. *Okuda* [1982] found a water side region of high vorticity near

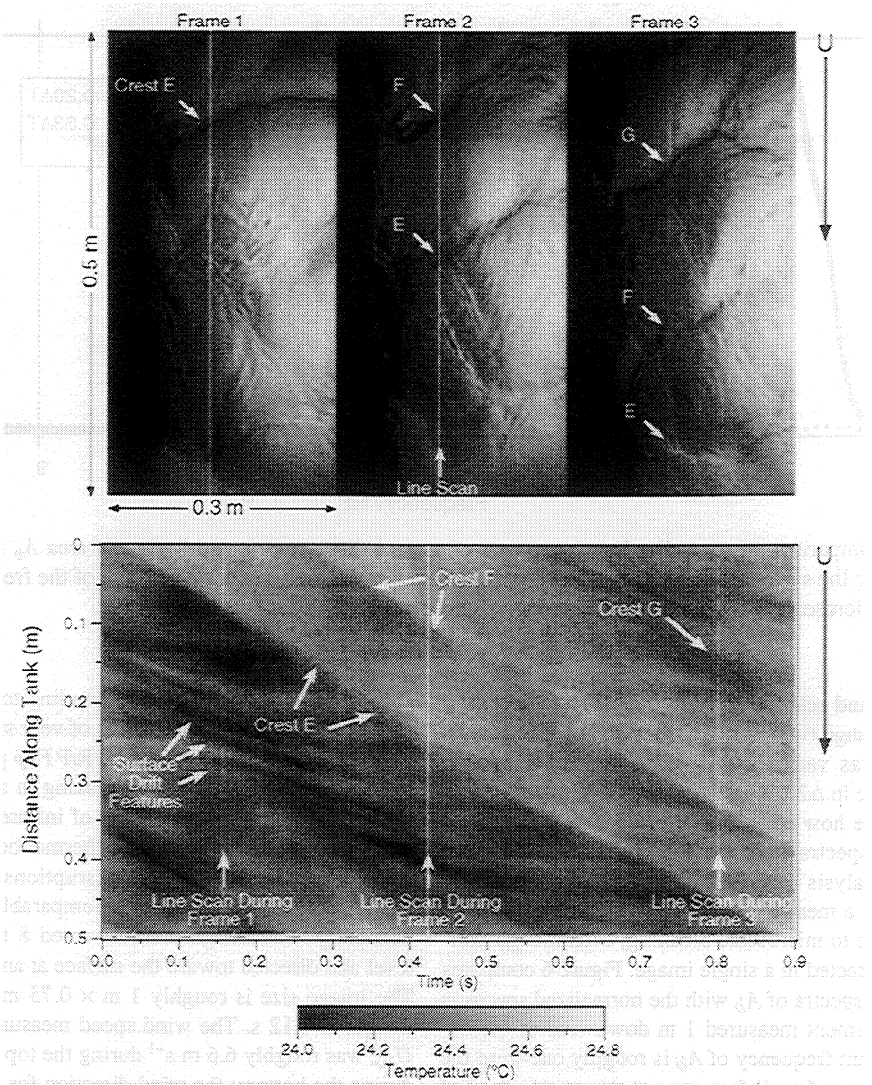

Figure 7. Example of measurements using the infrared imager to scan a single line oriented along the tank at a rate of 2500 Hz. (top) Sequence of video images showing the location of the line scan and three individual wave crests labeled E–G propagating along the tank. (bottom) Space-time plot of surface temperature spanning the time of the video images. The scan lines corresponding to the three video images are indicated. The disruption of the skin layer by each breaking crest appears as a sloping line which corresponds to $C_b = 0.5$ m s^{-1}. The warmer temperatures above these lines indicate that the skin layer is disrupted by the breaking crests; $T_w = 25.1$°C, $\Delta T_{aw} = -6.5$°C, RH = 49%, $f_p = 3.24$ Hz (measured at the test section), and $U = 8.1$ m s^{-1}.

crests that were occasionally accompanied by downward, subsurface bursts on the forward face.

Yoshikawa et al. [1988] used temperature as a passive tracer to detect these downward flows of water originating from the surface by combining fast response temperature measurements (at depths of 0.015, 0.035, and 0.072 m) and velocity measurements (at 0.072 m) in the near-surface layer under wind waves. The source of the tracer for the detection of downward flows was the cool skin layer, which was present owing to a net upward heat flux dominated by evaporation. Event-like temperature fluctuations of several millidegrees were coincident at all depths and occurred at intervals of the order of 10 s. These thermal intrusions were characterized by a rapid decrease in temperature followed by a more gradual recovery. The lifetime of roughly 10 s for the thermal events was much longer than the dominant wave period, which ranged from 0.24 to 0.36 s. The thermal events were correlated with increased downward and downwind velocity fluctuations which persisted for a similar duration. *Yoshikawa et al.* [1988] asserted that these low-frequency, large-scale features were due to downward bursts associated with individual wind waves, but the specific mechanism remained unresolved. The shallower thermistors showed far more rapid fluctuations, which suggests that the large-scale features detected by the deepest thermistor and the velocity sensor might be due to larger breaking events, or perhaps due to the additive effect of wave breaking in groups. These laboratory measurements provide direct evidence that fluid within the thermal sublayer is renewed by a turbulent process observed beneath wind waves.

The downward bursts reported by *Yoshikawa et al.* [1988] clearly were associated with individual waves and in all likelihood were produced by microscale wave breaking. While our observations indicate that not all waves are microscale breakers (as

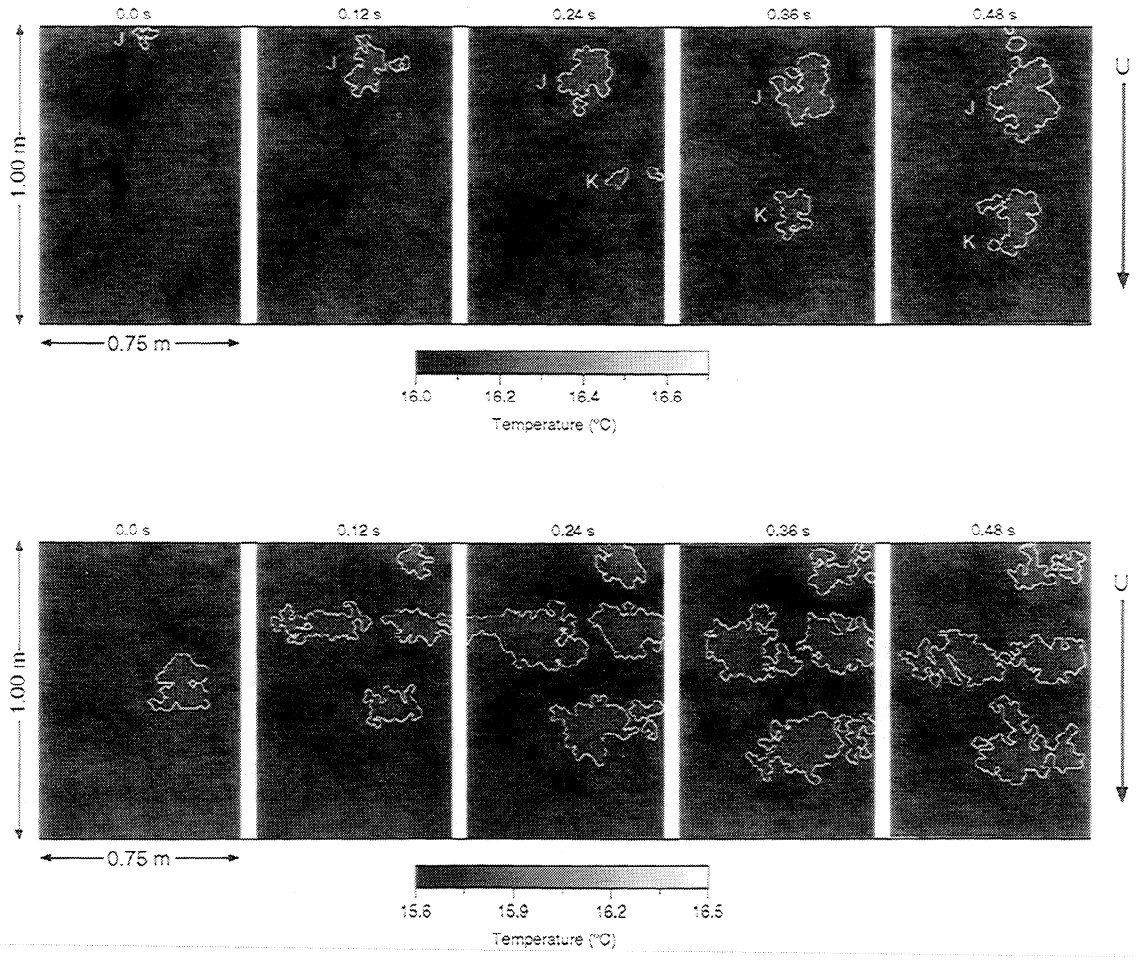

Figure 8. Nighttime sequences of infrared imagery demonstrating observations of microscale wave breaking aboard R/P *Flip* in September of 1995. The microscale breaking events within both sequences have been thresholded and outlined. These disruption events produce temperature changes of 0.1°C, which are comparable to an independently measured ΔT. (top) Evolution of a single event labeled J followed by the inception of a second event labeled K; U_{10} = 6.6 m s^{-1}, SWH = 2.28 m, f_{ps} = 0.070 Hz. (bottom) Example of multiple microscale breaking events; U_{10} = 5.7 m s^{-1}, SWH = 2.14 m, f_{ps} = 0.074 Hz. In both cases, the microscale breaking occurred as the orbital motion of long waves augmented the surface drift.

illustrated in Figure 9a), the frequency of microscale breaking we measure (about one-third the dominant wind-wave frequency) is significantly greater than the frequency of large-scale temperature intrusions reported by *Yoshikawa et al.* [1988]. The skin layer disruptions detected by the infrared imager represent renewal of the surface in the sense that the fluid parcels within 10 μm of the water surface overturn and are replaced by fluid parcels from below. Microscale wave breaking, for example, likely produces small-scale eddies that are sufficiently energetic to bring about surface disruption, as illustrated in Figure 9b. At times, however, a downward "bursting" motion may emerge as a result of a more intense microscale breaking event, as depicted in Figure 9c. We conclude that the reason for the difference between our results and those of *Yoshikawa et al.* [1988] is that not every microscale breaking wave produces a strong downward burst.

Komori et al. [1993] investigated the shear-induced turbulence under wind waves by considering it as the primary surface renewal mechanism for gas transfer, combining near-surface velocity measurements in both the air and water with gas flux measurements. Subsurface bursts near the wind wave crests, as well as more frequent "surface renewal motions," were observed to coincide with organized motions in the air. *Komori et al.* [1993] employed classical surface-renewal theory, which predicts the gas transfer velocity, k_L, based on the continuous random renewal of the laminar sublayer with the underlying water by turbulent eddies [*Danckwerts*, 1951]. The age of fluid elements occupying the surface, τ, is the timescale for surface renewal, which can be interpreted as the time scale for transport processes that occur at the air-sea interface. The gas transfer velocity is proportional to $(Ds)^{1/2}$, where D is the diffusivity of gas in water and $s = 1/\tau$ defines the surface renewal rate. According to theory, more intense turbulence increases the surface renewal rate and thus enhances the gas transfer. *Komori et al.* [1993] based s on the frequency of thresholded velocity fluctuations near the water surface, resulting in a surface renewal rate that was an order of magnitude greater than the wave frequency.

The velocity fluctuations that *Komori et al.* [1993] measured likely represent small-scale eddy motions produced primarily by microscale breaking waves. However, our measured frequency of microscale breaking is an order of magnitude less than the fre-

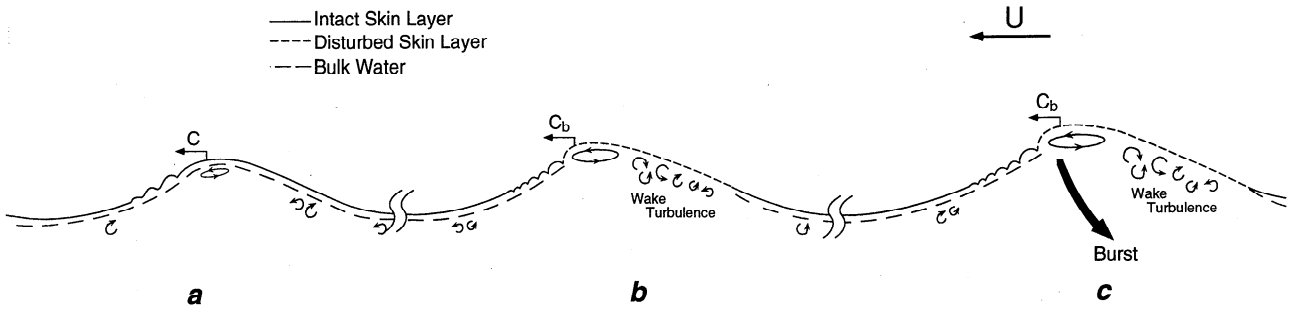

Figure 9. Illustration showing that not all wind waves are microscale breakers and not all microscale breaking waves produce bursts. (a) This wave is not a microscale breaker since the "roller" has not evolved into a "bore-like" crest which will disrupt the skin layer. (b) Microscale breaking produces small-scale eddies that are sufficiently energetic to bring about surface disruption. (c) Downward "bursting" motion may emerge as a result of a more intense microscale breaking event. The burst is shown for a reference frame moving with the crest. In general, no skin layer disruption will occur for eddies incapable of inducing fluid parcel overturning at the surface. Furthermore, not all turbulent eddies are due to microscale breaking events.

quency of surface renewal motions they used to estimate s. The length scale for the eddies measured by *Komori et al.* [1993] was of $O(0.01)$ m compared to the length scale of $O(0.1)$ m for the turbulent wakes of microscale breaking waves that we detect (see Figure 3). Therefore a probable reason for the difference between s measured by *Komori et al.* [1993] and the frequency of microscale breaking is the presence of multiple small-scale eddies within the turbulent wake of a single microscale breaking event. Another potential contributing factor is that not all small-scale eddies near the surface correspond directly to microscale breaking events. The line scan measurements, like those in Figure 7, do not show high-frequency skin layer disruptions in areas unaffected by microscale breaking. In all likelihood, not all of the eddies in these areas were capable of producing skin layer disruption by fluid-parcel overturning at the surface because of the suppression of vertical motion by the density discontinuity at the air-water interface. Our findings highlight that the frequency of microscale breaking is distinctly different from the surface renewal rate, $s = 1/\tau$, used in traditional surface renewal models that are based on shear-induced turbulence.

Models of the gas transfer velocity have evolved into a consistent formulation which may be expressed as

$$k_L = \beta u_* Sc^{-n} \tag{1}$$

where β is a dimensionless constant, u_* is the water-side friction velocity, and Sc is the Schmidt number, given by $Sc = \nu/D$ (where ν is the kinematic viscosity of the water). An exponent of $n = 1/2$ is consistent with classical surface-renewal theory. While parameterizations of the exchange of heat [*Wick et al.*, 1996] and gas [*Jähne et al.*, 1987] using surface renewal theory have had some success, fundamental differences between the classical idea of surface renewal and the influence of waves remain to be reconciled in modeling these air-sea fluxes. For instance, *Jähne et al.* [1987] reported that k_L increases linearly with the total mean square wave slope, which suggests that deficiencies in gas transfer models and discrepancies among laboratory and field results may be overcome by considering wave-related parameters. The established importance of waves to gas transfer, combined with the surface disruption due to microscale breaking waves demonstrated here, implies that microscale wave breaking may indeed be a likely mechanism for enhancing k_L.

The work by *Csanady* [1990] to model the effect of microscale wave breaking on gas flux resulted in (1) with $n = 1/2$ and $\beta = \alpha\varepsilon$, where α is a dimensionless constant and ε is the fractional surface area covered by wave-induced divergences, that is, where the diffusion boundary layer becomes thin as a result of microscale breaking waves. *Csanady* [1990] estimated a value of at least 0.20 for ε based on measurements reported by *Jähne et al.* [1987]. While the values of A_b in Figure 5 are consistent with *Csanady*'s [1990] estimate for ε, a meaningful comparison will require measurements over a wide range of wind speeds at varying fetch. *Csanady*'s [1990] instructive modeling work provides a point of reference for future descriptions of gas transfer incorporating microscale wave breaking. In addition to ε, one might expect k_L to depend on other parameters that characterize microscale breaking, such as the rate of recovery of the affected area and the size and intensity distribution of surface disruptions.

Details of the formation and evolution of a breaking wave crest have recently emerged both in theory [*Longuet-Higgins*, 1992, 1994; *Longuet-Higgins and Cleaver*, 1994] and experiment [*Duncan et al.*, 1994]. The infrared space-time plot in Figure 7 indicates that our present infrared capabilities combined with improved video measurements will provide unprecedented details of the microscale breaking process, such as the exact location of initial surface disruption. The images in Figure 8 of microscale breaking in the presence of swell show that infrared techniques can be used to detect enhanced microscale breaking due to long-wave/short-wave interaction. Preferential breaking of very short gravity waves along the phase of long waves has been suggested as the mechanism responsible for modulation of the skin temperature by swell waves [*Jessup and Hesany*, 1996]. In the area of microwave remote sensing, recent modeling of radar backscatter has been based on scattering from either the bore-like crest [*Trizna and Carlson*, 1996] or the parasitic capillaries [*Plant*, 1997] of microscale breaking waves.

4. Concluding Remarks

Microscale breaking waves disrupt the skin layer and produce thermal surface signatures that can be quantified by infrared imaging techniques. As far as we know, these are the first published measurements of the infrared signature of microscale breaking

waves. The infrared techniques we have outlined provide a new and objective measurement method for identifying and quantifying microscale breaking waves despite their low visual contrast and small scale. Furthermore, our observations suggest that the infrared signature of microscale wave breaking may serve as a practical means of defining the phenomenon itself.

We have demonstrated the ability to obtain the frequency of occurrence and the areal coverage of microscale wave breaking. The limited measurements presented here show that the fractional area of water surface affected by microscale wave breaking can be substantial under a moderately forced laboratory wind wave field. The frequency of microscale wave breaking was roughly one-third that of the dominant wave. Evidence from the literature suggests that downward "bursting" phenomena observed beneath laboratory wind waves are likely produced by microscale wave breaking. However, the frequency of microscale wave breaking we measure is significantly higher than the frequency of bursting reported by others, implying that not all microscale breaking waves produce these "bursts." Other readily available quantities of interest include the rate of recovery, the intensity, and the duration of microscale wave breaking events. Examples of ocean measurements demonstrated that these techniques may also be applied in the field. Infrared techniques should provide the quantitative measurements necessary to incorporate microscale wave breaking into models of heat and gas flux at the air-sea interface. Moreover, extraordinary details on the origin and evolution of microscale breaking waves are provided by infrared techniques.

Acknowledgments. We thank M. G. Skafel of the National Water Research Institute, Canada Centre for Inland Waters (CCIW), and M. R. Loewen of the University of Toronto for the opportunity to work at CCIW. We thank R. Kropfli and C. Fairall for the opportunity to participate in the Coastal Ocean Processes Experiment as well as the crew of R/P *Flip* for the assistance received during the field operation. We thank V. Hesany of the Applied Physics Laboratory at the University of Washington (APL-UW) and R. K. Schiff for laboratory assistance. This work was funded by grants from the Office of Naval Research, the National Aeronautics and Space Administration, and APL-UW.

References

Banner, M. L., and D. H. Peregrine, Wave breaking in deep water, *Annu. Rev. Fluid Mech., 25*, 373–397, 1993.

Banner, M. L., and O. M. Phillips, On the incipient breaking of small scale waves, *J. Fluid Mech., 65*, 647–656, 1974.

Csanady, G. T., The role of breaking wavelets in air-sea gas transfer, *J. Geophys. Res., 95*, 749–759, 1990.

Danckwerts, P. V., Significance of liquid-film coefficients in gas absorption, *Ind. Eng. Chem., 43*, 1460–1467, 1951.

Donelan, M., M. S. Longuet-Higgins, and J. S. Turner, Periodicity in whitecaps, *Nature, 239*, 449-451, 1972.

Duncan, J. H., V. Philomin, M. Behres, and J. Kimmel, The formation of spilling breaking water waves, *Phys. Fluids, 6*, 2558–2560, 1994.

Ebuchi, N., H. Kawamura, and Y. Toba, Fine structure of laboratory wind-wave surfaces studied using an optical method, *Boundary Layer Meteorol., 39*, 133–151, 1987.

Gemmrich, J., and L. Hasse, Small-scale surface streaming under natural conditions as effective in air-sea gas exchange, *Tellus, Ser. B, 44*, 150–159, 1992.

Jähne, B., K. O. Munnich, R. Bosinger, A. Dutzi, W. Huber, and P. Libner, On the parameters influencing air-water gas exchange, *J. Geophys. Res., 92*, 1937–1949, 1987.

Jessup, A. T., and V. Hesany, Modulation of ocean skin temperature by swell waves, *J. Geophys. Res., 101*, 6501–6511, 1996.

Jessup, A. T., C. J. Zappa, V. Hesany, M. R. Loewen, and M. G. Skafel, Dependence of the skin layer recovery rate on heat flux and turbulence, in *Air-Water Gas Transfer*, edited by B. Jähne and E. C. Monahan, pp. 601–610, Aeon, Hanau, Germany, 1995.

Jessup, A. T., C. J. Zappa, M. R. Loewen, and V. Hesany, Infrared remote sensing of breaking waves, *Nature, 385*, 52–55, 1997.

Katsaros, K. B., The aqueous thermal boundary layer, *Boundary Layer Meteorol., 18*, 107–127, 1980.

Kawamura, H., and Y. Toba, Ordered motion in the turbulent boundary layer over wind waves, *J. Fluid Mech., 197*, 105–138, 1988.

Kitaigorodskii, S. A., On the fluid dynamical theory of turbulent gas transfer across an air-sea interface in the presence of breaking wind-waves, *J. Phys. Oceanogr., 14*, 960–972, 1984.

Komori, S., R. Nagaosa, and Y. Murakami, Turbulence structure and mass transfer across a sheared air-water interface in wind-driven turbulence, *J. Fluid Mech., 249*, 161–183, 1993.

Longuet-Higgins, M. S., Capillary rollers and bores, *J. Fluid Mech., 240*, 659–679, 1992.

Longuet-Higgins, M. S., Shear instability in spilling breakers, *Proc. R. Soc. London, Ser. A, 446*, 399–409, 1994.

Longuet-Higgins, M. S., and R. P. Cleaver, Crest instabilities of gravity waves, 1, The almost-highest wave, *J. Fluid Mech., 258*, 115–129, 1994.

Melville, W. K., The role of surface-wave breaking in air-sea interaction, *Annu. Rev. Fluid Mech., 28*, 279–321, 1996.

Okuda, K., Internal flow structure of short wind waves, I, On the internal vorticity structure, *J. Oceanogr. Soc. Jpn., 38*, 28–42, 1982.

Phillips, O. M., and M. L. Banner, Wave breaking in the presence of wind drift and swell, *J. Fluid Mech., 66*, 625–640, 1974.

Plant, W. J., A model for microwave Doppler sea return at high incidence angles: Bragg scattering from bound, tilted waves, *J. Geophys. Res.*, in press, 1997.

Robinson, I. S., N. C. Wells, and H. Charnock, The sea surface thermal boundary layer and its relevance to the measurement of sea surface temperature by airborne and spaceborne radiometers, *Int. J. Remote Sens., 5*, 19–45, 1984.

Saunders, P. M., The temperature at the ocean-air interface, *J. Atmos. Sci., 24*, 269–273, 1967.

Thorpe, S. A., Dynamical processes of transfer at the sea surface, *Prog. Oceanogr., 35*, 315–352, 1995.

Toba, Y., M. Tokuda, K. Okuda, and S. Kawai, Forced convection accompanying wind waves, *J. Oceanogr. Soc. Jpn., 31*, 192–198, 1975.

Trizna, D. B., and D. J. Carlson, Studies of dual polarized low grazing angle radar sea scatter in nearshore regions, *IEEE Trans. Geosci. Remote Sens., 34*, 747–757, 1996.

Wick, G. A., W. J. Emery, L. H. Kantha, and P. Schlüssel, The behavior of the bulk-skin sea surface temperature difference under varying wind speed and heat flux, *J. Phys. Oceanogr., 26*, 1969–1988, 1996.

Yeh, H. H., Vorticity generation at a fluid interface, in *Breaking Waves*, edited by M. L. Banner and R. H. J. Grimshaw, pp. 257–265, Springer-Verlag, New York, 1992.

Yeh, H. H., Free-surface dynamics, in *Advances in Coastal Engineering*, edited by P. L.-F. Liu, pp. 1–74, World Scientific, 1995.

Yoshikawa, I., H. Kawamura, K. Okuda, and Y. Toba, Turbulent structure in water under laboratory wind waves, *J. Oceanogr. Soc. Jpn., 44*, 143–156, 1988.

A. T. Jessup and C. J. Zappa, Applied Physics Laboratory, University of Washington, 1013 N.E. 40th Street, Seattle, WA 98105-6698. (e-mail: jessup@apl. washington. edu, zappa@apl.washington.edu)

H. Yeh, Department of Civil Engineering, University of Washington, Seattle, WA 98195-2700. (e-mail: harryeh@u.washington.edu)

(Received December 9, 1996; revised April 28, 1997; accepted May 15, 1997.)